Available online at www.sciencedirect.com
SCIENCE DIRECT
Earth and Planetary Science Letters 242 (2006) 354–364
EPSL
www.elsevier.com/locate/epsl

Evidence for an earthquake barrier model from Mw ~ 7.8 Kokoxili (Tibet) earthquake slip-distribution

Y. Klinger [a,*], R. Michel [b], G.C.P. King [a]

[a] Tectonique, Institut Physique du Globe de Paris, BP89, 4 place Jussieu, 75005 Paris, France
[b] Lab. Détection et de Géophysique, CEA, BP12, 91680 Bruyères-le-Châtel, France

Received 8 September 2005; received in revised form 30 November 2005; accepted 2 December 2005
Available online 18 January 2006
Editor: V. Courtillot

Abstract

The slip distribution of the Mw ~ 7.8 Kokoxili (Tibet, 2001) earthquake has been measured at high resolution using optical correlation of satellite images and provides both the parallel and perpendicular components of the horizontal co-seismic slip. This reveals a variation of the horizontal slip at a scale of ~ 20 km along-strike. Anti-correlation of slip parallel and perpendicular to the fault indicates transfer of slip from the horizontal to the vertical component at the ends of segments. These features suggest a rupture model with segments separated by strong persistent geometric barriers. The unexpected ending of the rupture south of the main fault can be explain by such a structure but bears important implications for the initiation and rupture directivity of the next earthquake.

Keywords: earthquake rupture; fault mechanics; Kunlun fault

1. Introduction

Dynamic rupture studies of earthquakes adopt different views of the relation between the propagating rupture and fault geometry. On one hand, the asperity concept [1] where the rupturing part of fault plane is described as the "stronger" or more stressed part of the fault, and on the other hand the barrier concept [2] where tough [3] and hence stressed regions delimit the parts of the fault that ruptures. In this view, the ruptured fault segment is regarded as less "strong". The barriers arrest rupture and, in extreme cases, stop it [4]. In the asperity model, large earthquakes form when several neighbouring asperities rupture consecutively. There is little reason why the slip-distribution associated with this model should reflect observed fault segmentation. In the barrier model, the rupture initiates on one segment and propagates to the neighboring segments, either unilaterally or bilaterally, having to pass barriers between each segment. In this case, barriers are associated with identifiable fault features such as bends or offsets and the signature of the barrier should be visible in the slip-distribution associated with the earthquake [5].

Although such features have been identified from mapping surface rupture [6], seismic, Insar and GPS data lack the resolution to distinguish between the models [7]. Most field measurements of rupture carried out after large earthquakes are either spatially too

* Corresponding author.
E-mail addresses: klinger@ipgp.jussieu.fr (Y. Klinger), remi.michel@cea.fr (R. Michel).

0012-821X/$ - see front matter © 2006 Elsevier B.V. All rights reserved.
doi:10.1016/j.epsl.2005.12.003

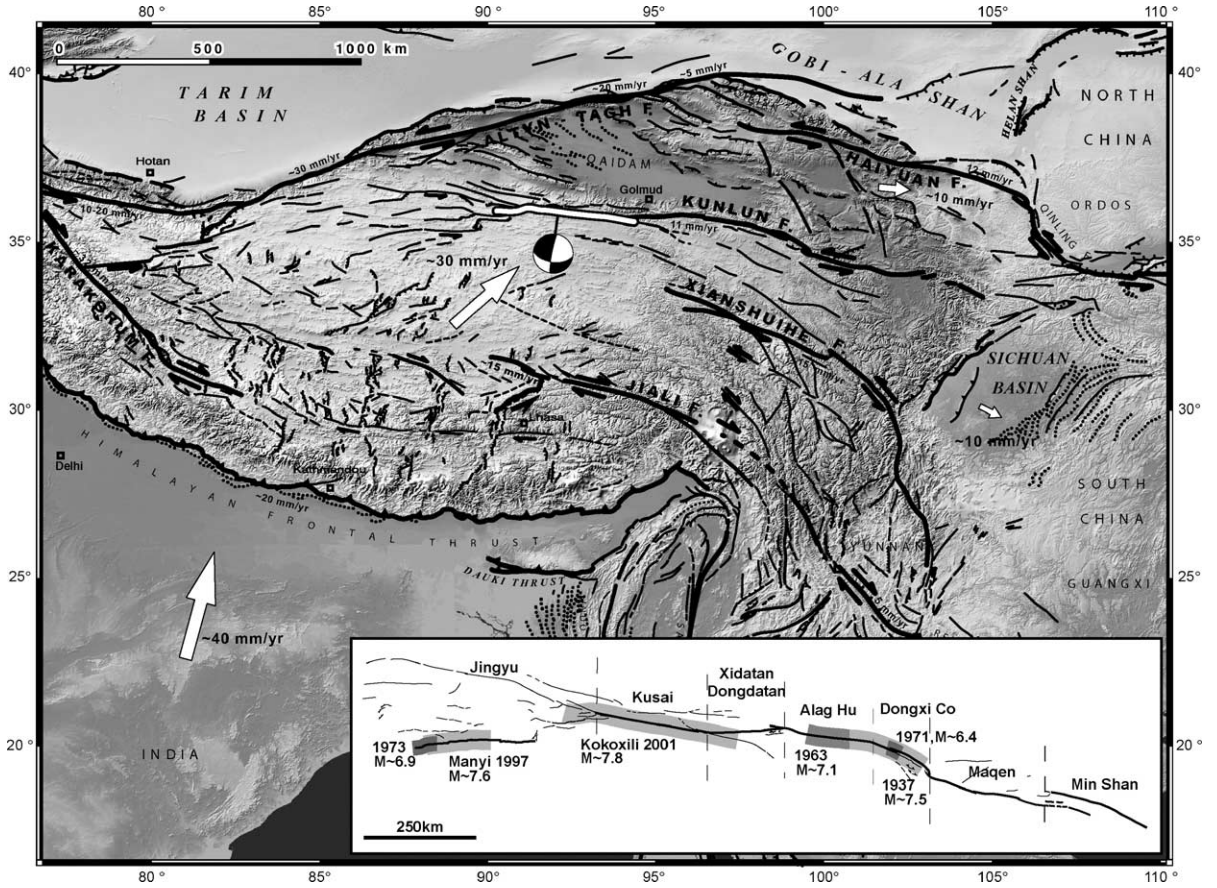

Fig. 1. Main active faults of the Tibetan part of the India–Asia collision zone (modified from [10]). The 450-km-long rupture of the Mw ~7.8 Kokoxili earthquake (14 November 2001) is outlined in white, with centroid focal sphere (Harvard). Inset shows earthquake dislocations along the Kunlun fault since 1930, emphasizing the very long rupture length of the 14 November 2001 earthquake and the seismic gap along the Xidatan-Dongdatan segment (different shades are used to distinguish between overlapping ruptures).

limited [8] or too sparse along strike [9], preventing the relation between slip-variations and segmentation (10–30 km) to be clearly identified. Here, we correlate optical images to study the surface rupture of the Mw ~7.8 Kokoxili (Tibet) event (Fig. 1), and provide observations that support the barrier model for earthquake rupture.

2. Kokoxili earthquake ruptures

The Kokoxili event triggered a flurry of studies because it provided a unique opportunity to study a giant continental earthquake in an arid environment where surface features are not masked by vegetation. This earthquake occurred along the western end of the Kunlun fault (Fig. 1). This fault is one of the major left-lateral strike-slip faults that allow extrusion of the Tibet plateau eastward [10]. The slip-rate along the Kunlun fault has been estimated to be about 1 cm/yr based on independent geologic [11] and GPS [12] studies. A detailed description of the rupture and the geodynamic context has already been published (see [13] and references herein) and only salient features are summarized below.

The rupture initiated in a pull-apart basin (N35°57′/E90°32.4′, Fig. 2), and propagated ~50 km along the western section and for ~400 km to the east along the extensional corridor, the Kusai section and the Kunlun Pass section. The rupture, in the extensional corridor was oriented about 20° CCW relative to the Kusai section. Surface expression of the rupture is not well developed along this part. From the point where the rupture joined the Kusai section (N36°01.35′/E90°14.32′), it propagated eastward for ~270 km without any major change in strike. At the end of the Kusai section (N35°43.8′/E93°39′) instead of following the Xidatan fault, generally regarded as the main strand of the Kunlun fault eastward [11] the rupture continued on the Kunlun Pass section where it propagated for a

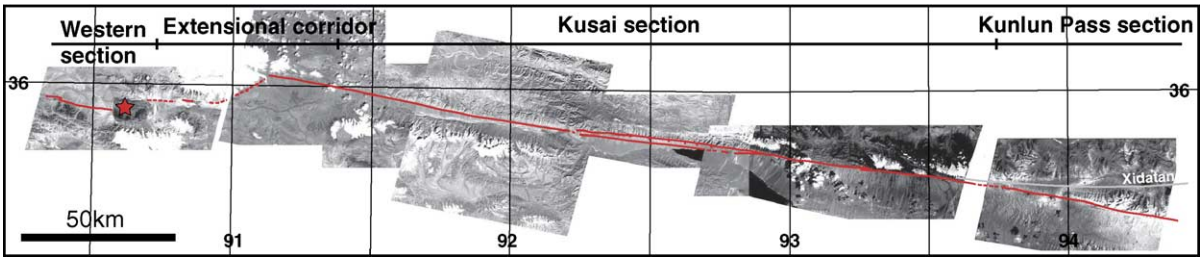

Fig. 2. Spot mosaic covering the entire 2001 earthquake rupture. Epicentre and surface ruptures are indicated.

further ~70 km. This last section displays a modest thrust component in addition to the strike-slip component. The average co-seismic slip associated with the 2001 earthquake is 2 to 3 m with a maximum slip of ~10 m.

3. Optical image correlation

Maps of ground displacement and associated uncertainties are computed from subpixel correlation of optical images acquired by the SPOT satellites before and after the earthquake [14–16]. This technique yields robust estimates of the rupture geometry and of the two components of horizontal displacement near the fault, parallel and perpendicular to the co-seismic rupture. It complements SAR interferometry that often fails near the fault due to excessive temporal decorrelation of the images and signal saturation. Furthermore, SAR data only provide the satellite to ground component of the deformation [15]. Thus, the study in this paper, which shows the relation between the two horizontal components, cannot be accomplished using SAR.

We processed 8 pairs (Table 1) of Spot images covering ~400 km of rupture and measured the displacements with an accuracy of ~1 m, every 320 m.

Fig. 3A, B and C show, respectively, the degree of correlation and the map of horizontal offset along *x*- and *y*-axes. Loss of coherence within the western and extensional sections, characterized by a snowy pattern in the correlation image, prevents reliable offset measurements there. In the western section, the co-seismic rupture lies on the northern front of the mountain range (Fig. 2). The fault trace is hardly discernable from the limit between the coherent patch, to the south, which corresponds to the mountain range, and the zone of low coherence, to the north, which is associated with unstable alluvial surfaces (alluvial fan, river bed, etc.). This prevents useful offset measurement, although fieldwork has shown that offset can locally reach 4 m [13]. The corridor section, affected by several active drainages, does not display a coherent signal either. From the western end of the Kusai section eastward, the trace of the co-seismic rupture is very sharp. Changes in azimuth (A on Fig. 3B) and relay zones (B on Figs. 3B and 4) can be identified. The Kunlun Pass fault section is characterized by a higher decorrelation probably due to larger snow coverage and glaciers. Nevertheless, the trace of the rupture (C on Fig. 3B and boxes indicating location of Fig. 8) is clearly visible just north of the range front, which is responsible for a small residual topographic signal. The trace of the co-seismic rupture along the *y*-axis is subdued (Fig. 3C), in keeping with the dominant strike-slip behavior of the East–West oriented Kunlun fault. Any significant signal observed along the *y*-axis corresponds to the projection of some vertical motion on the horizontal plane, in the case of extensional or compressional jogs for example. Such deformation, ubiquitous along the whole rupture, is responsible for the faint co-seismic trace visible in Fig. 3C.

Offsets maps include bias induced by instrumental uncertainties (view parameters, optics and detection) and by the correlation procedure [14]. For SPOT

Table 1
List of spot images used to compute correlation maps

Platform	Date (DD.MM.YYYY)	Reference (K–J)	Incidence (Left/Right degree)
SPOT–3	3.8.1996	230–278	L 8.30
SPOT–4	7.4.2004	230– 277	R 5.00
SPOT–3	5.11.1996	231–278	R 2.30
SPOT–4	22.7.2003	231–277	R 0.30
SPOT–3	5.11.1996	232–278	L 2.30
SPOT–4	8.10.2003	232–278	L 2.50
SPOT–1	29.10.1989	233–278	L 4.60
SPOT–4	30.11.2002	233–278	L 4.50
SPOT–1	12.6.1988	234–278	R 4.60
SPOT–4	24.10.2003	234–277	R 5.70
SPOT–4	22.1.2003	235–278	R 20.30
SPOT–1	15.5.1998	235–278	R 21.60
SPOT–4	28.8.2002	236–278	L 25.40
SPOT–2	31.8.1992	236–278	L 26.20
SPOT–4	17.6.2002	238–278	L 6.90
SPOT–2	2.10.1992	237–278	L 5.90

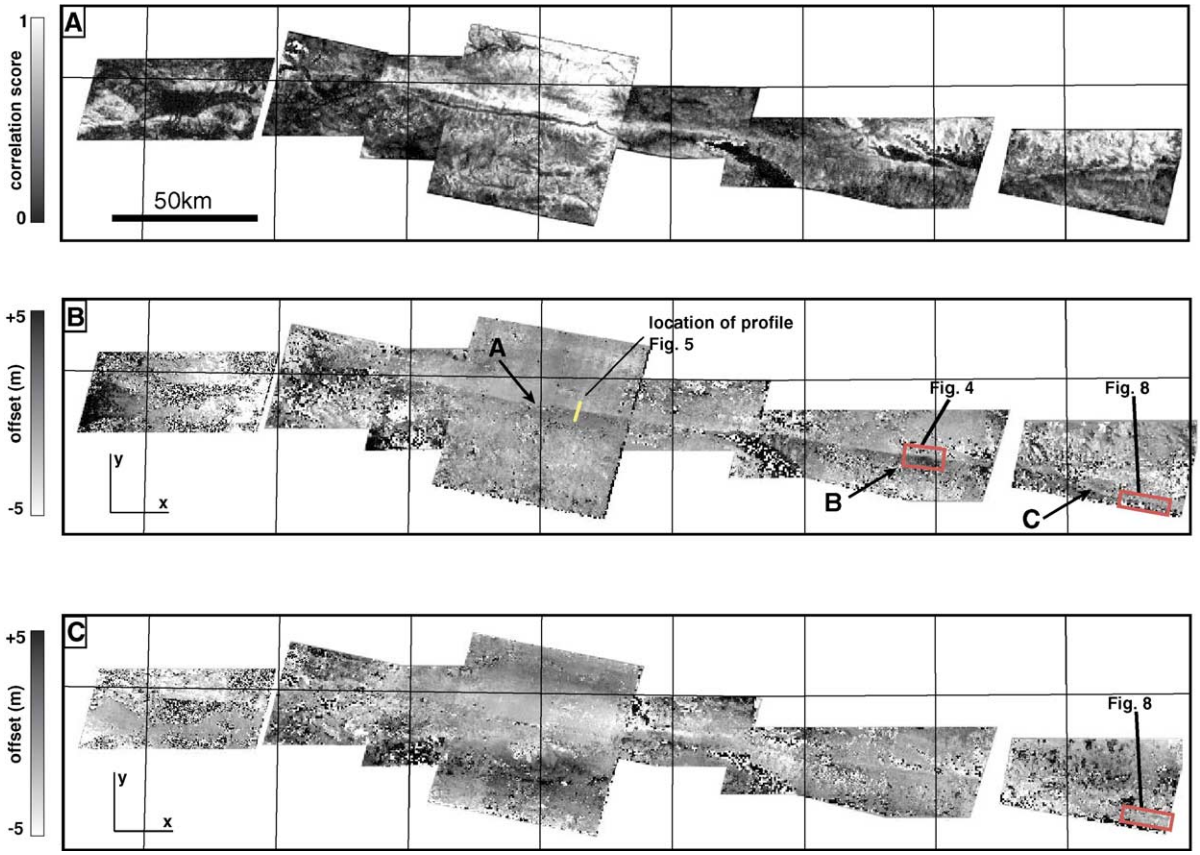

Fig. 3. (A) Map of the correlation score. Loss of coherence within the western and extensional sections, characterized by a snowy pattern in the correlation image, prevents reliable offset measurements there. (B) Map of offset along the *x*-axis direction. Motion eastward is positive. (C) Map of offset along the *y*-axis direction. Motion southward is negative.

imagery, it has been demonstrated that bias is scale dependant, yielding pluri-metric errors at the 5 km^{-1} scale or below and error of few tens of centimetres at the 100 m^{-1} scale or above [14]. This prevents estimates of low spatial frequency patterns of ground deformation, but has no influence on slip estimates from profiles across the fault [17] (Fig. 5). Offsets may also suffer from residual topographic errors resulting from uncertainties in Digital Elevation Models and on stereoscopic angles. Using SRTM DEM and SPOT imagery and the procedure describe by [14], this source of uncertainty is estimated to be as high as 107 cm (rms) for correlation windows 640 m × 640 m in size in a highly mountainous area. Fortunately, this noise is reduced to about 21 cm within the relatively flat area (alluvial fans and bajada) ruptured by the earthquake.

Fault offsets are then estimated every kilometre from the amplitude of the discontinuity on stacked profiles, weighted by correlation score, perpendicular to the fault (Fig. 5). Accuracy of offset is limited by this local correlation score (Fig. 3A).

Slip estimated from profiles mainly includes noise from temporal decorrelation of the images and offset gradients within the correlation window. Calibrated uncertainties on measurement are derived from the correlation score [14]. Uncertainty of slip from a raw profile is typically slightly below 1/10th of the pixel size (1 m on the ground) for correlation windows 640 m × 640 m in size, but may increase to 1 pixel within highly decorrelated area (Fig. 3A). The resulting uncertainty in slip decreases with the resolution in a near square-root-n form down to about 34.4 cm (rms) for slip estimated with independent measurement every 5 km (Fig. 6).

4. Discussion

Fig. 6 shows the slip-curve projected parallel and perpendicular to the local strike of the fault. Acknowledging that the Kunlun fault accommodates almost pure strike-slip displacement, the component of slip measured perpendicular to the fault corresponds to

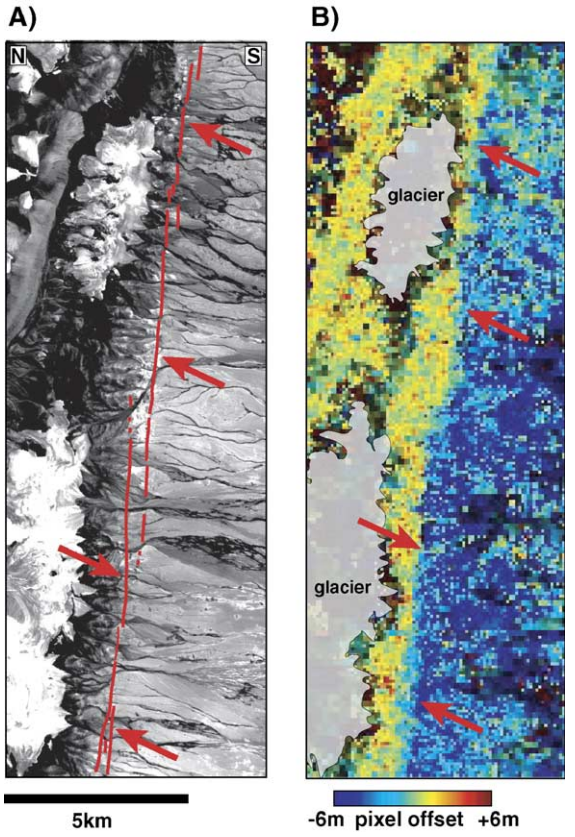

Fig. 4. Close-up views of measurements showing details of the co-seismic rupture in a relay zone. (A) Extract of post-earthquake Spot image. The surface rupture is outlined in red. (B) Corresponding correlation image measured in the direction parallel to the rupture. Red arrows point to the co-seismic rupture.

projection onto the horizontal direction of vertical motion (up or down) on dipping faults (Fig. 7). The average slip along strike (Fig. 6A) is 2.7 m with 2 maximum peaks reaching ~8 m with, on average, no slip perpendicular to the fault (Fig. 6B), although locally it can reach large positive or negative values, reflecting local geometric complexities. The Kunlun Pass section is characterized by a lower slip, ~0.6 m. Interestingly, the eastern part of the Kulun Pass section shows a more coherent pattern with a systematic motion southward (Fig. 8). The average horizontal motion is ~1.7 m. This could result from 1.96 m slip occurring on a 30° dipping fault. This is consistent with the thrust component of the Kunlun Pass section reported from field observation [18]. Our results show overall good agreement with the slip-curve extrapolated from InSar data [19]. Comparison with offset data measured in the field [20] also shows general good agreement. Interestingly, places where field data clearly are larger than offsets we measured from optical correlation, are places where larger dispersion of the field data is observed. The western end of the Kusai section provides a good example where offsets from optical correlation yield values between 2 m and 3 m, in good agreement with Insar data [19]. At the same place, field data range from 2 m to 6 m. It seems very probable to us that some cumulative offsets have been misinterpreted to be 2001 offsets as in some cases it could be tricky to distinguish between single and cumulative offset due to earthquake [13]. This interpretation is supported by the fact that the largest values measured in such place are almost twice as large of the lower values collected in the same place, in good agreement with characteristic-slip models [21,22].

The moment magnitude Mw corresponding to the slip-distribution we measured was computed using a crust 15 km thick [19,23] and slip-values from correlation data where reliable data exist and an average horizontal slip of 2 m for the western section, based on field observations [13]. The shear modulus was assumed to be 3×10^{11} dyn/cm^2. The extensional corridor was not included because no surface slip distribution is available. This gives a Mw ~ 7.7, in good agreement with the magnitude estimated from other methods. This suggests that the slip distribution at the surface is compatible with the actual motion on the fault plane and that no major slip occurred at depth that did not reach the surface, unlike for smaller earthquakes [24,25].

The slip-curves presented here allow us to discuss the relation between segmentation of the fault and surface rupture. Although these relations were already

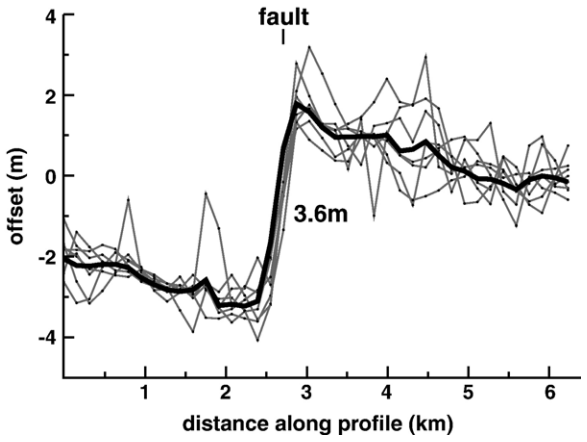

Fig. 5. Raw profiles (gray) extracted from the parallel component offset map (see Fig. 3B for location). Profiles are measured each 160 m along fault for 1 km and stacked (bold line) to reduce noise. Seismic offset is measured from the stacked profile.

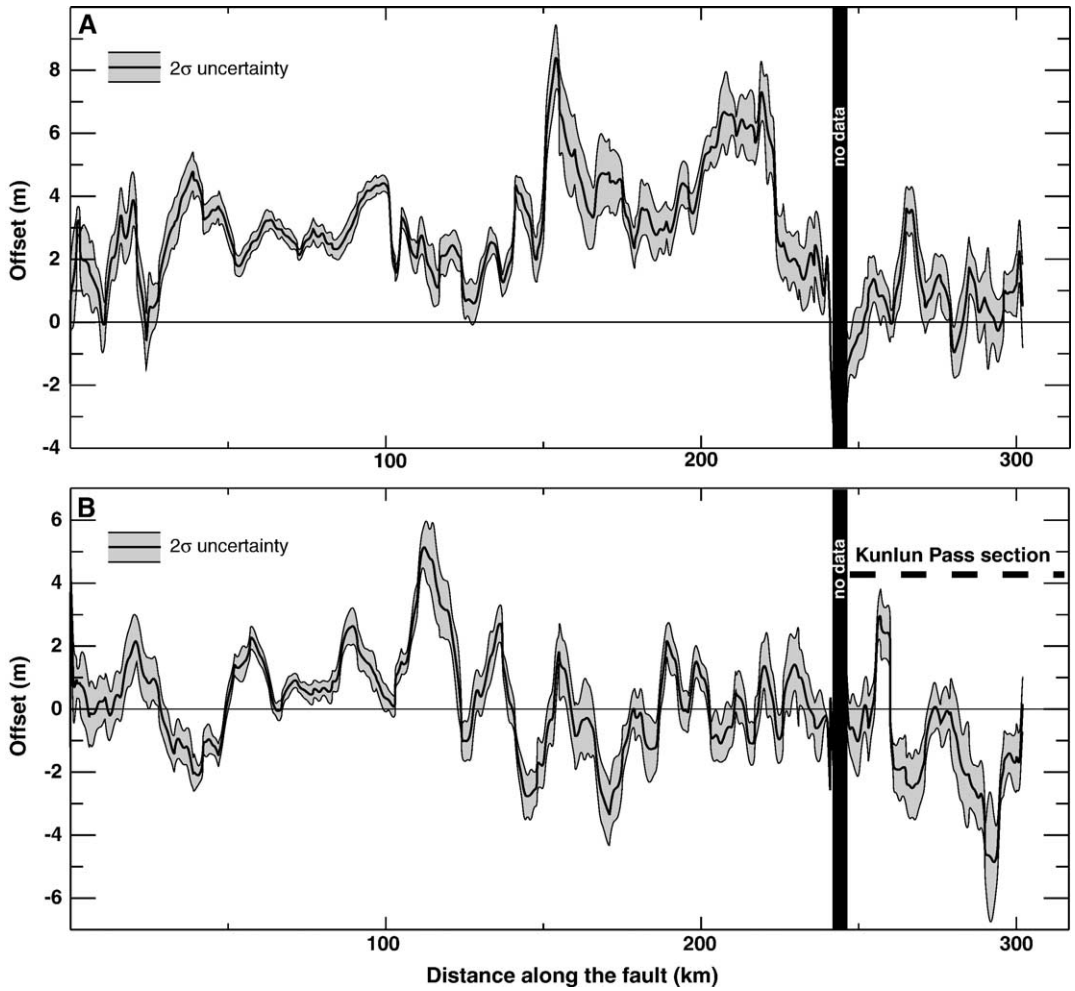

Fig. 6. (A) Displacement parallel, along *x*-axis, (A) and normal, along *y*-axis, (B) to the fault measured from stacked profiles averaged over 5 km along fault. Left-lateral and northward motion is positive. Local azimuth of the rupture is measured directly from Spot images acquired after the event.

suggested from seismic data (e.g. [4]) and field observations (e.g. [6]), measurements of slip, both parallel and perpendicular to the rupture were not possible. Fig. 9 shows the slip distribution in the direction parallel to the rupture. The slip-distribution consists of short segments, 15 to 25 km long (average length 14.9 km), that display bumps of larger slip. The edges of the sections are marked by low points in the slip curve. Although spatial resolution is lower, inversion based on Insar data shows that variations of slip are not only due to surficial effect but could be extended at depth [19]. Fig. 9 shows the map of the rupture associated with the Kokoxili earthquake, derived from field exploration and satellite image interpretation. The location of the jogs (compressional and extensional) that were activated during the event are indicated in red. Side faults that connect to the main rupturing fault are in light grey. Almost without exception low slip zones match the location of jogs, bends or a junction with side faults. The slip-distribution is clearly related to the geometrical structure of the fault. Field investigation has shown that most of these features

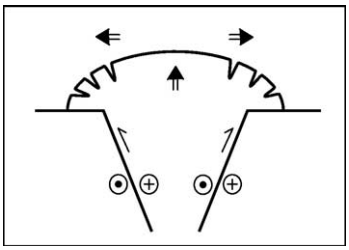

Fig. 7. In compressional or extensional jogs vertical motion generates displacement perpendicular to the fault.

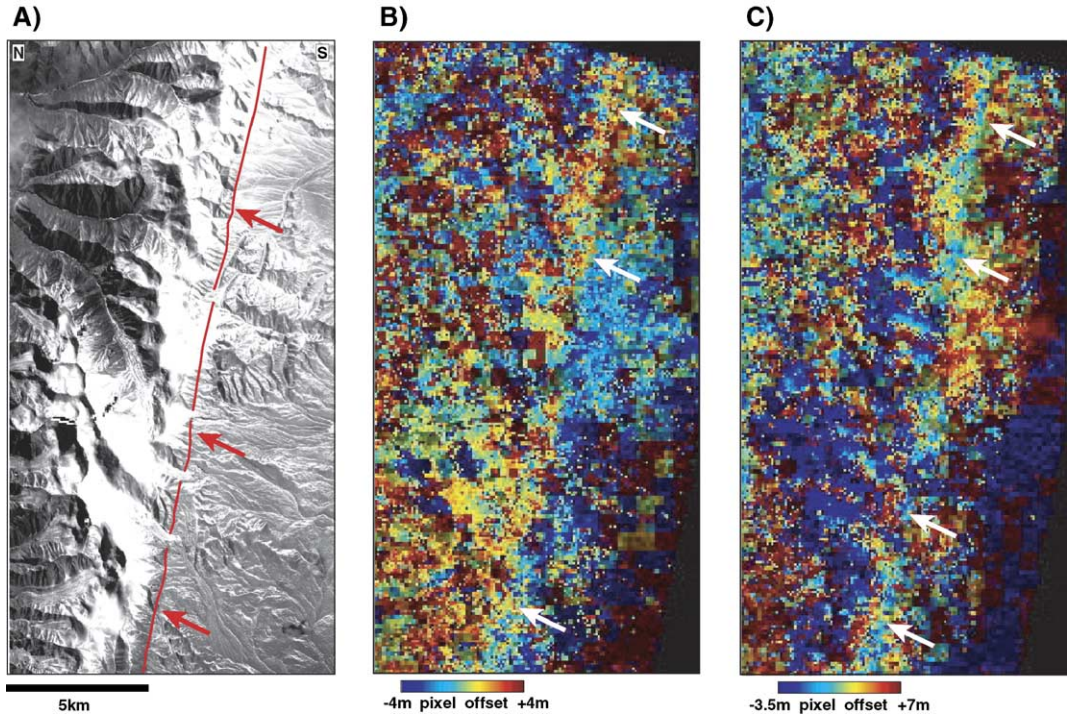

Fig. 8. Close-up views of measurements showing details of the co-seismic rupture along the Kunlun Pass section where thrust has been observed in addition to strike-slip motion. (A) Extract of post-earthquake Spot image. The surface rupture is outlined in red. (B) Correlation image measured in the direction parallel to the fault. White arrows point to the trace of the strike-slip motion. (C) Correlation image measured in the direction perpendicular to the fault. Systematic motion southward indicated by white arrows corresponds to the projection of the thrust component of the motion onto the horizontal plane, detectable by optical correlation.

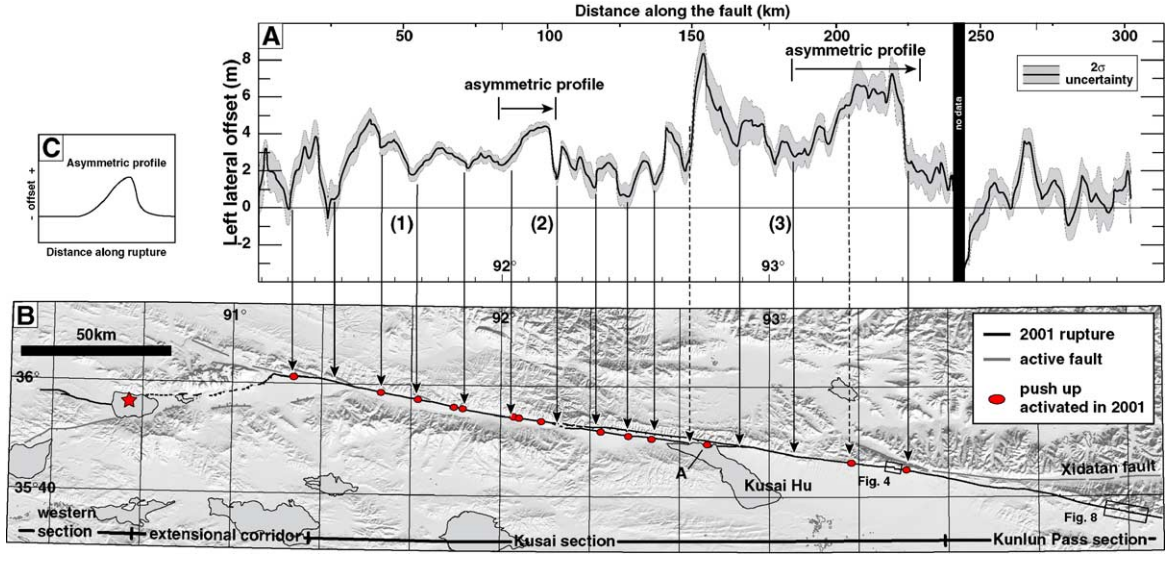

Fig. 9. (A) Slip measured parallel to the fault (left-lateral motion is positive). The slip is derived from correlation of Spot images averaged over 5 km along rupture. (B) Map of the 2001 event surface ruptures. Red star locates earthquake epicenter. (C) Asymmetric profile is characterized by slow rising of the slip value followed by a sharp drop. Local minima of the slip-curve correspond (black arrows), with two exceptions (dashed arrows), to geometric barriers like push-ups (1), fault branching (2) or changes of fault azimuth (3) identified along the fault. At least two asymmetric slip profiles can be identified that are unambiguously associated to split of the fault trace.

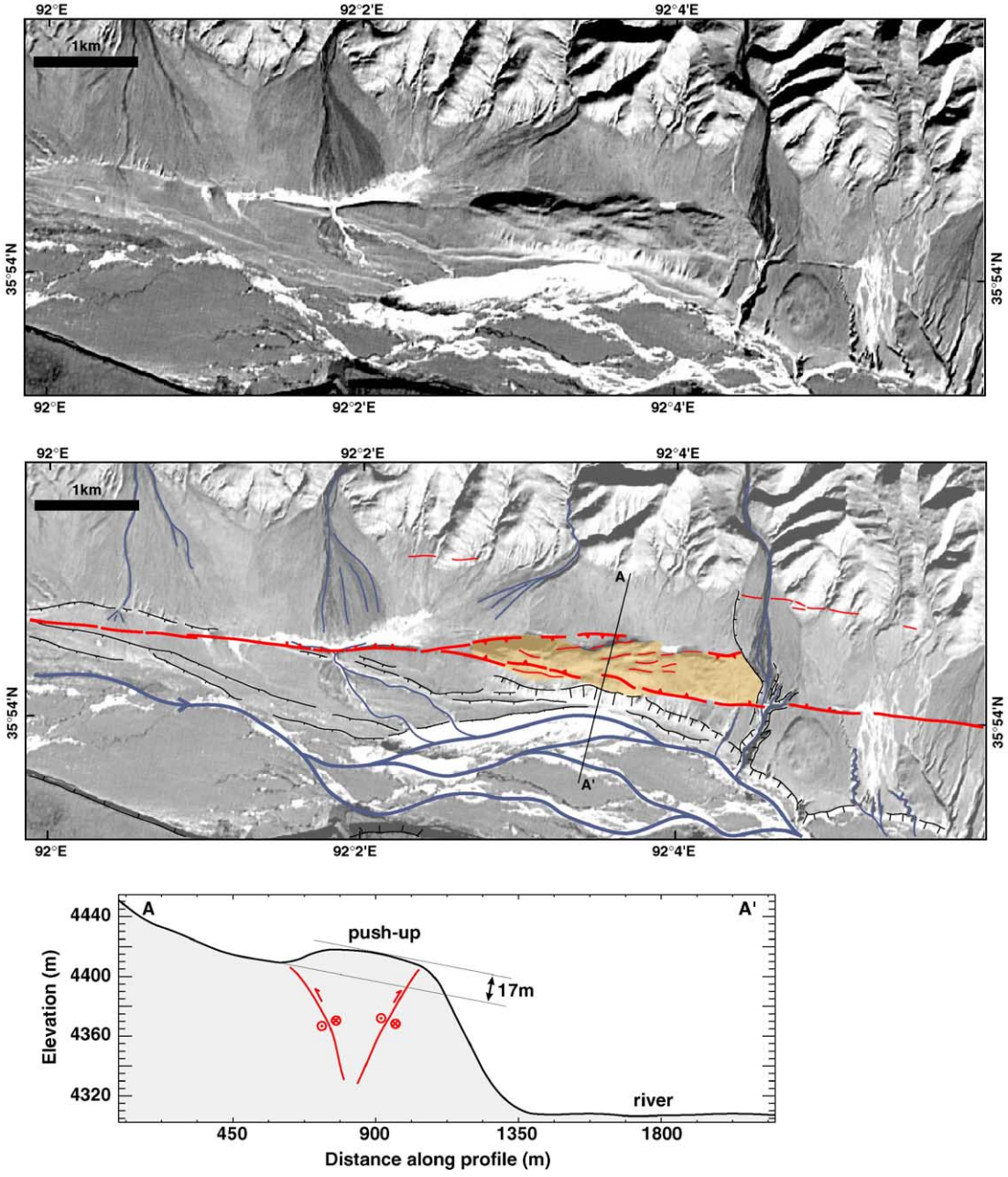

Fig. 10. Satellite image of a typical push-up along the Kusai section activated during the 2001 earthquake. The horizontal motion transfers to vertical in the relay zone. The size of this ridge shows that it has been active for several seismic cycles.

have been activated and apparently played a similar role in many previous earthquakes (Fig. 10). It is worth noting that the pull-apart basin on the northern shore of the Kusai Hu (A in Fig. 9) does not affect the slip-distribution in a visible way. The slip seems to be most affected by compressive jogs or side faults connecting to the rupturing fault [26]. Fig. 11 shows the coefficient of cross-correlation between the slip measured parallel to and perpendicular to the fault, computed for a lag of ±50 km. For lag values close to zero, the coefficient is significant [27] and negative indicating anti-correlation between the motion on the two components.

This behaviour is to be expected for a geometric barrier where the slip is accommodated on a multitude of small faults distributed through a wide range of scales and orientations that differ from that of the main fault

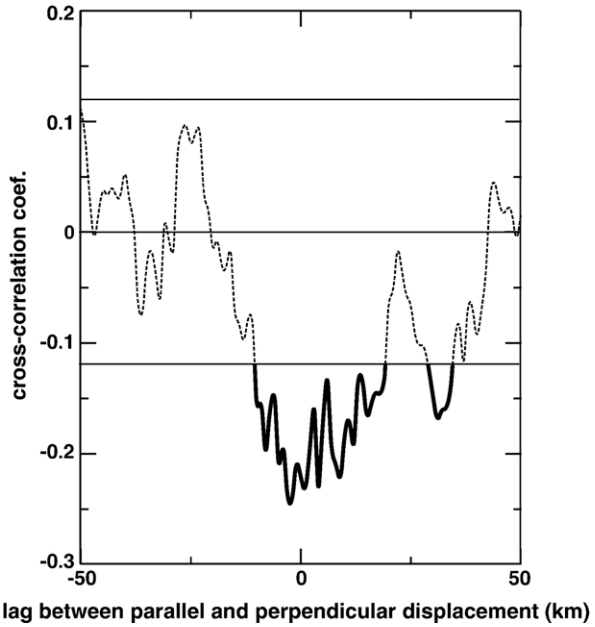

Fig. 11. Cross-correlation between displacement measured parallel and perpendicular to the fault along the Kusai section. The bold line indicates where the coefficient is significantly different from zero. The minimum around zero indicates anti-correlation of the two components of motion.

[28]. Such barrier geometry favours the transfer of horizontal motion to vertical motion that is visible on the component perpendicular to the fault (Figs. 3C and 8). Compressive jogs and junctions between different fault segments are most favourable places for such behaviour.

Some barriers are tough enough to stop the rupture propagation and force the fault system to activate other segments to allow further propagation of the rupture. In a normal faulting context, cumulative slip-curves with linear increase ending in a sharp drop have been identified as specific signature of such barriers [29]. A similar signature has also been suggested for the 1979 Imperial fault strike-slip earthquake [30]. Such patterns can be recognized in at least two places along the Kokoxili rupture (Fig. 9). In both cases, the slip distribution is highly asymmetrical. In the western case, slip rises smoothly from 2 m to 4 m in about 15 km and drops abruptly to less than 2 m in few km. The decrease is associated (Fig. 9) with the onset of the slip-partitioning section [31] where the rupture splits into two parallel branches. In the eastern case, slip increases progressively eastward from 2 m to 7 m over ~50 km, to drop abruptly to 2 m in ~10 km (Fig. 9). This rapid decrease is associated with the triple junction where the rupturing fault meets with the, as yet, unbroken Xidatan segment and an additional side fault connecting from the north. At this point, the rupture propagated southward along the Kunlun Pass fault instead of the Xidatan section. We suggest that the junction between the eastern termination of the Kusai section and the western part of the Xidatan section forms a tough barrier. This barrier stopped the rupture abruptly. Some short discontinuous cracks located in the first kilometre of the Xidatan fault perhaps indicate an aborted attempt to trigger rupture along the Xidatan fault. As no clear connection between the Kusai section and the Xidatan fault exists, it was apparently easier for the rupture to transfer to the better oriented Kunlun Pass fault, although it is only a secondary feature at regional scale [11]. Once the rupture started along the Kunlun Pass fault, the western end of the Xidatan fault was immediately affected by the stress shadow of the

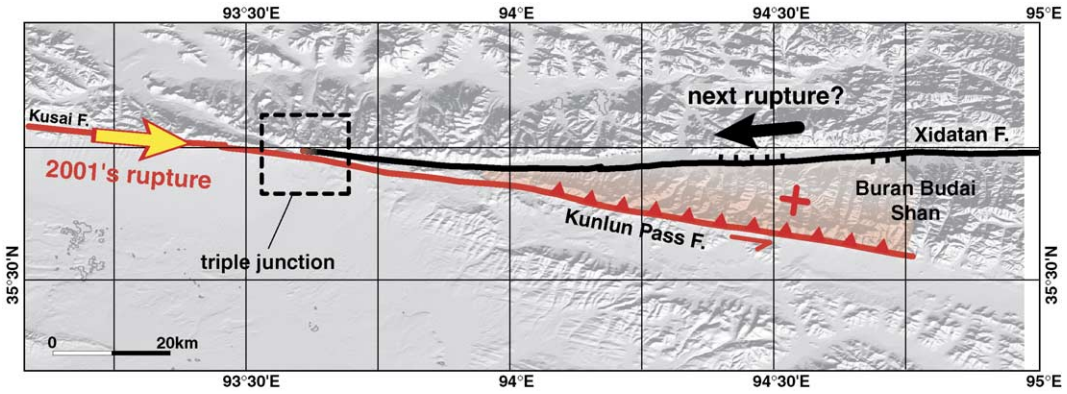

Fig. 12. Field observation shows no clear connection between Kusai and Xidatan Faults. Earthquake rupture propagated preferably along the Kunlun Pass Fault, whose azimuth requires a thrust component to explain the growth of the Buran Budai Shan. A stress shadow due to the 2001 rupture minimises chances for future earthquake to initiate at the western end of the Xidatan Fault, and favours propagation from the east and ending at the triple junction.

current rupture [32], impeding any further triggering along the Xidatan fault. The thrust component along the Kunlun Pass fault partially reduced the normal stress along the Xidatan fault and brought it closer to failure. However, the absence of a real connection between Kusai section and Xidatan fault and the stress shadow due to the 2001 rupture at this barrier make the next earthquake along the Xidatan fault unlikely to start at this barrier and suggests that the next rupture along Xidatan fault will initiate farther east and propagate westward (Fig. 12).

With few exceptions, the barriers identified along the 2001 Kokoxili rupture correspond to compressive jogs or changes in azimuth of the fault trace. The average length of the segments delimited by the barriers is 14.9 km. Almost no very large continental strike-slip earthquake has been documented in a similar way to the Kokoxili earthquake. However, reasonable maps and offset data have been published for the Haiyuan Mw ~ 8 earthquake in 1920 [33] and the Luzon Mw ~ 7.8 earthquake in 1990 [34], with rupture lengths of ~ 120 km and ≥ 120 km, respectively, and maximum horizontal slip larger than 5 m in both cases. Study of the segmentation reveals that these two cases again show average segment lengths of 15–20 km. Morphological mapping of the southern San Andreas fault, also exhibits similar segment scaling [35] although not directly correlated to specific events. Finally, indirect evidences from seismology support these observations. A signature visible in the power spectrum of accelerograms recorded for large earthquakes corresponds to breaking segments with lengths of the order of 10 to 30 km [36].

5. Conclusion

Based on the new high resolution and unambiguous observations from the Kokoxili earthquake, we propose, following earlier suggestions, that the length of the seismic segments is limited by barriers, which are geometric in nature. Although faults have a broadly self-similar geometry [37] segment regularity appears at scales of 15–20 km which we speculate is related to the thickness of the seismogenic crust. The clear support that our observations provide to the Aki model has major implications for modelling the dynamics of earthquake rupture [38].

Acknowledgments

This paper benefits from fruitful discussions with P. Tapponnier. We thank S. Dominguez and an anonymous reviewer for constructive comments. Spot data were acquired through ISIS Program of CNES. This is IPGP contribution number 2109 and INSU contribution number 389.

References

[1] H. Kanamori, G. Stewart, Seismological aspects of the Guatemala Earthquake of February 4, 1976, Journal of Geophysical Research 83 (B7) (1978) 3427–3434.
[2] S. Das, K. Aki, Fault plane with barriers: a versatile earthquake model, Journal of Geophysical Research 82 (1977) 5658–5669.
[3] C. Scholz, The Mechanics of Earthquakes and Faulting, Cambridge University Press, New York, 1990. 439 pp.
[4] K. Aki, Characterization of barriers on an earthquake fault, Journal of Geophysical Research 84 (1979) 6140–6148.
[5] E.M. Dunham, P. Favreau, J.M. Carlson, A supershear transition mechanism for cracks, Science 299 (2003) 1557–1559.
[6] G.C.P. King, G. Yielding, The evolution of a thrust fault system: processes of rupture initiation, propagation and termination in the 1980 El Asnam (Algeria) earthquake, Geophysical Journal Royal Astronomic Society 77 (1984) 915–933.
[7] S. Peyrat, R. Madariaga, K. Olsen, La dynamique des tremblements de terre vue à travers le séisme de Landers du 28 juin 1992, Comptes Rendus de l'Academie des Sciences, Mecanique 330 (2002) 1–14.
[8] S. McGill, C. Rubin, Surficial slip distribution on the central Emerson fault during the June 28, 1992, Landers earthquake, Journal of Geophysical Research 104 (B3) (1999) 4811–4834.
[9] P.J. Haeussler, D.P. Schwartz, T.E. Dawson, H.D. Stenner, J.J. Lienkaemper, B. Sherrod, F.R. Cinti, P. Montone, P.A. Craw, A.J. Crone, S.F. Personius, Surface rupture and slip distribution of the Denali and Totschunda faults in the 3 November 2002 M 7.9 earthquake, Alaska, Bulletin of the Seismological Society of America 94 (6) (2004) S23–S52.
[10] P. Tapponnier, X. Zhiqin, F. Roger, B. Meyer, N. Arnaud, G. Wittlinger, Y. Jingsui, Oblique stepwise rise and growth of the Tibet plateau, Science 294 (2001) 1671–1677.
[11] J. Van Der Woerd, P. Tapponnier, F.J. Ryerson, A.S. Meriaux, B. Meyer, Y. Gaudemer, R.C. Finkel, M.W. Caffee, G.G. Zhao, Z.Q. Xu, Uniform postglacial slip-rate along the central 600 km of the Kunlun Fault (Tibet), from Al-26, Be-10, and C-14 dating of riser offsets, and climatic origin of the regional morphology, Geophysical Journal International 148 (3) (2002) 356–388.
[12] Q. Wang, P. Zhang, J.T. Freymueller, R. Bilham, K.M. Larson, X. Lai, X. You, Z. Niu, J. Wu, Y. Li, J. Liu, Z. Yang, Q. Chen, Present-day crustal deformation in China constrained by global positioning system measurements, Science 294 (2001) 574–577.
[13] Y. Klinger, X. Xu, P. Tapponnier, J. Van Der Woerd, C. Lasserre, G.C.P. King, High-resolution satellite imagery mapping of the surface rupture and slip distribution of the Mw 7.8, November 14, 2001 Kokoxili earthquake (Kunlun fault, northern Tibet, China), Bulletin of the Seismological Society of America 95 (5) (2005) 1970–1987.
[14] N. Van Puymbroeck, R. Michel, R. Binet, J.P. Avouac, J. Taboury, Measuring earthquakes from optical satellite images, Applied Optics 39 (20) (2000) 3486–3494.
[15] R. Michel, J.P. Avouac, Deformation due to the 17 August 1999 Izmit, Turkey, earthquake measured from Spot images, Journal of Geophysical Research 107 (B4) (2002).

[16] S. Dominguez, J.P. Avouac, R. Michel, Horizontal coseismic deformation of the 1999 Chi-Chi earthquake measured from Spot satellite images: implications for the seismic cycle along the western foothills of central Taiwan, Journal of Geophysical Research 108 (B2) (2003), doi:10.1029/2001JB000951.
[17] R. Michel, J.P. Avouac, Imaging co-seismic fault zone deformation from air photos: the Kickapoo stepover along the surface ruptures of the 1992 Landers earthquake, Journal of Geophysical Research (in press).
[18] X. Xu, W. Chen, W. Ma, G. Yu, G. Chen, Surface rupture of the Kunlunshan earthquake (Ms 8.1), northern Tibetan plateau, China, Seismological Research Letters 73 (6) (2002) 884–892.
[19] C. Lasserre, G. Peltzer, F. Crampe, Y. Klinger, J. Van Der Woerd, P. Tapponnier, Coseismic deformation of the 2001 Mw=7.8 Kokoxili earthquake in Tibet, measured by SAR interferometry, Journal of Geophysical Research 110 (B12408) (2005), doi:10.1029/2004JB003500.
[20] J. Chen, Y. Chen, G. Ding, Z. Wang, Q. Tian, G. Yin, X. Shan, Z. Wang, Surficial slip distribution and segmentation of the 426-km-long surface rupture of the 14 November, 2001, Ms8.1 earthquake on the east Kunlun fault, northern Tibetan plateau, China, Seismology and Geology 26 (3) (2004) 378–392 (in Chinese with English abstract).
[21] J. Liu, Y. Klinger, K. Sieh, C. Rubin, Six similar sequential ruptures of the San Andreas fault, Carrizo Plain, California, Geology 32 (8) (2004) 649–652.
[22] K. Sieh, The repetition of large-earthquake ruptures, Proceedings of the National Academy of Sciences 93 (1996) 3764–3771.
[23] M. Antolik, R.E. Abercrombie, G. Ekstrom, The 14 November 2001 Kokoxili (Kunlunshan), Tibet, earthquake: rupture transfer through a large extensional step-over, Bulletin of the Seismological Society of America 94 (4) (2004) 1173–1194.
[24] G.C.P. King, C. Vita-Finzi, Active folding in the Algerian earthquake of 10 October 1980, Nature 292 (5818) (1981) 22–26.
[25] Y. Fialko, D. Sandwell, M. Simons, P. Rosen, Three-dimensional deformation caused by the Bam, Iran, earthquake and the origin of shallow slip deficit, Nature 435 (19) (2005) 295–299.
[26] G.C.P. King, Speculations on the geometry of the initiation and termination processes of earthquake rupture and its relation to morphology and geological structures, Pure and Applied Geophysics 124 (3) (1986) 567–585.
[27] C. Chatfield, The Analysis of Time Series, Chapman and Hall, London, 1989.
[28] G.C. King, J. Nabelek, The role of fault bends in faults in the initiation and termination of earthquake rupture, Science 283 (1985) 984–987.
[29] I. Manighetti, G.C.P. King, C.G. Sammis, The role of off-fault damage in the evolution of normal faults, Earth and Planetary Science Letters 217 (2004) 399–408.
[30] S. Ward, Dogtails versus rainbows: synthetic earthquake rupture models as an aid in interpreting geological data, Bulletin of the Seismological Society of America 87 (1997) 1422–1441.
[31] G. King, Y. Klinger, D. Bowman, P. Tapponnier, Slip partitioned surface breaks for the 2001 Kokoxili earthquake, China (Mw 7.8), Bulletin Seismological Society America 95 (2) (2005) 731–738.
[32] G.C.P. King, M. Cocco, Fault interaction by elastic stress changes: new clues from earthquake sequences, Advances in Geophysics 44 (2001) 1–38.
[33] Institut of Geology and Ninxia Bureau of seismology, Active Haiyuan fault Zone Monograph, Seismological Publishing House, Beijing, China, 1990 286 pp.
[34] T. Nakata, H. Tsutsumi, R.S. Punongbayan, R.E. Rimando, J. Daligdig, A. Daag, G.M. Besana, Surface Fault Ruptures of the 1990 Luzon Earthquake, Philippines, Hiroshima University Special Pub, Hiroshima, Japan, 1996.
[35] R. Bilham, P. Williams, Sawtooth segmentation and deformation processes on the southern San Andreas fault, California, Geophysical Research Letters 12 (1985) 557–560.
[36] A.A. Gusev, Descriptive statistical model of earthquake source radiation and its application to an estimation of short-period strong motion, Geophysical Journal Royal Astronomic Society 74 (1983) 787–808.
[37] G.C.P. King, The accommodation of large strains in the upper lithosphere of the Earth and other solids by self-similar fault systems: the geometrical origin of b-value, Pure and Applied Geophysics 121 (1983) 761–1093.
[38] M.R. Handy, G. Hirth, N. Hovius, The dynamic of fault zones, in: M.R. Handy, G. Hirth, N. Hovius (Eds.), Dahlem Workshop 95, MIT Press, Berlin, 2005.